Biosensors and Bioelectronics 78 (2016) 236–243

Contents lists available at ScienceDirect

Biosensors and Bioelectronics

journal homepage: www.elsevier.com/locate/bios

Highly sensitive electrochemical sensing platform for lead ion based on synergetic catalysis of DNAzyme and Au–Pd porous bimetallic nanostructures

Qian Zhou, Youxiu Lin, Yuping Lin, Qiaohua Wei *, Guonan Chen, Dianping Tang *

Key Laboratory of Analysis and Detection for Food Safety (Ministry of Education & Fujian Province), Institute of Nanomedicine and Nanobiosensing, Department of Chemistry, Fuzhou University, Fuzhou 350108, PR China

ARTICLE INFO

Article history:
Received 6 September 2015
Received in revised form
16 November 2015
Accepted 17 November 2015

Keywords:
Electrochemical biosensor
Lead ion
Bimetallic nanoparticles
DNAzyme

ABSTRACT

In this work, a sensitive and specific electrochemical biosensor for lead ion (Pb^{2+}) detection was developed by coupling with synergetic catalysis of porous Au–Pd bimetallic nanoparticles and hemin/G-quadruplex-based DNAzyme. In the presence of target Pb^{2+}, the substrate strand was cleaved and the enzyme strand was released. Subsequently, G-rich DNA-labeled Au–Pd bimetallic nanoparticle was linked with the released enzyme strand through the helper DNA. Upon addition of hemin, a large number of hemin/G-quadruplex-based DNAzyme molecules were formed on the electrode to serve as nicotinamide adenine dinucleotide hydrogen (NADH) oxidase and peroxidase mimics. DNAzyme could catalyzed the reduction of H_2O_2, generated from NADH in the presence of O_2, to produce an electrochemical signal when using thionine as the electron mediator. Introduction of porors Au–Pd bimetallic nanoparticles could enhance the detectable signal and cause the increase in the sensitivity. Experimental results showed that the variations (ΔI) in the cathodic peak currents of the biosensor were linearly dependent on target Pb^{2+} concentrations from 1.0 pM to 100 nM with a detection limit (LOD) of 0.34 pM. The excellent performance of the sensing platform indicated its promising prospect as a valuable tool for simple and cost-effective Pb^{2+} detection in practical application.

1. Introduction

Due to the serious impacts on ecosystem and high toxicity to human health, heavy metal ions have become major environmental contaminants found in air, soil and drinking water (Gao et al., 2012; Bontidean et al., 2003). Among them, lead ion (Pb^{2+}, one of the most toxic environmental pollutants) can be toxic even at low concentrations. More unfavorably, its accumulation in human body can also cause diverse detrimental effects on human health, *e.g.*, anemia, nervous system dysfunction and reproductive dysfunction (Tsekenis et al., 2015; He et al., 2013a; Li et al., 2012; Qian et al., 2015). Considering the severe toxicity of lead ion, developing sensitive and selective strategies for Pb^{2+} detection has been of great concern in the past decades as well as recent years. To this end, techniques such as inductively coupled plasma mass spectrometry (ICP-MS) (Mitrano et al., 2012), atomic absorption spectrometry (Naghmush et al., 1995), colorimetric (Dwivedi et al., 2015), fluorescent (Kuo et al., 2015), electrochemiluminescent (Li et al., 2015) and electrochemical (Dong et al., 2015) methods have been developed for Pb^{2+} detection. Nevertheless, most protocols involved in the complex experimental procedures and high cost (*e.g.*, enzymes or expensive equipments), thus limiting their practical routine application. In contrast, electrochemical sensors have been widely used because of their high sensitivity, low cost and fast response (Shen et al., 2008; Muralikrishna et al., 2014; Zhang et al., 2015a).

DNAzymes are catalytic DNA sequences obtained by *in-vitro* selection, which have been widely utilized for highly sensitive detection of various target analytes, *e.g.*, metal ions, DNA and small molecules (Zhang et al., 2015b; Liu et al., 2015; Guo et al., 2015). 8-17 DNAzyme (as a typical kind of DNAzymes) is a DNA metalloenzyme catalyzing RNA transesterification in the presence of divalent metal ions (Liu et al., 2015). As for Pb^{2+}-dependent DNAzyme comprising of enzyme strand and substrate stand, the substrate strand can be cleaved into two pieces in the presence of target Pb^{2+}. Hemin-bound G-quadruplex is another DNAzyme with peroxidase-like activity, and the formed mechanism is described in detail in the literatures (Ruttkay-Nedecky et al., 2013;

* Corresponding authors.
E-mail addresses: qhw76@fzu.edu.cn (Q. Wei), dianping.tang@fzu.edu.cn (D. Tang).

http://dx.doi.org/10.1016/j.bios.2015.11.055
0956-5663/

Chung et al., 2015; Ma et al., 2015; Han et al., 2014). Typically, hemin/G-quadruplex can catalyze H_2O_2-mediated oxidation of reductive substrates including 3,3′,5,5′-tetramethylbenzidine and luminol (Zhang et al., 2015c; He et al., 2013b). Recent studies demonstrated that hemin/G-quadruplex could also act as the NADH oxidase (Golub et al., 2011; Yuan et al., 2013). In this regard, hemin/G-quadruplex can be employed as the NADH oxidase and peroxidase-mimicking DNAzyme simultaneously, thereby avoiding the labeling natural enzymes. With the oxidation of NADH to co-factor NAD^+, H_2O_2 is formed in the meantime because of hemin/G-quadruplex toward NADH catalysis. Subsequently, the hemin/G-quadruplex can undertake peroxidase-like mimic to catalyze the reduction of newly generated H_2O_2 and H_2O_2-mediated oxidation of reductive substrates to produce the signal.

Owing to the advantages including large surface coverage and unique electronic/catalytic properties, many nanomaterials have been applied to improve the sensitivity of the detection methods (Li et al., 2014; Lin et al., 2014). Inspiringly, noble metal nanostructures (*e.g.*, gold nanoparticle, AuNP and palladium nanoparticle, PdNP) have attracted much attention because of their excellent biocompatibility and catalytic performance (Bukar et al., 2014; Poon et al., 2014). In contrast, bimetallic nanostructures have been usually utilized for design of various sensing platforms due to the enhanced chemical, physical and prominent catalytic properties in comparison with their corresponding monometallic components (Yuan et al., 2014; Gui and Jin, 2013). In mechanical terms, such the nanocomposites differ from conventional composite materials owing to the exceptionally high surface-to-volume ratio of the reinforcing phase and /or the exceptionally high aspect ratio (Zhang et al., 2011). Au–Pd bimetallic nanoparticles (one kind of the bimetallic nanomaterials) have gained great attraction for the unique catalytic properties (Cheng et al., 2012). Upon effective electronic coupling effects of the constituents, Au–Pd bimetallic hybrid nanostructures exhibited the enhanced catalytic activities compared with AuNP or PdNP alone (Gao and Goodman, 2012). In this case, Au–Pd hybrid nanoscales can not only be applied for immobilization of biomolecules, but also be employed to catalyze the reduction of H_2O_2 (Ge et al., 2014), thereby endowing its adoption to fabricate sensitive electrochemical sensing platforms.

Herein, we design a sensitive sensing platform for Pb^{2+} detection based on the synergetic catalysis of hemin/G-quadruplex-based DNAzyme and Au–Pd porous bimetallic nanoparticles (Scheme 1). First, Pb^{2+}-specific DNAzyme comprising of enzyme strand and substrate strand is immobilized on a cleaned gold electrode *via* the Au–S bond. In the presence of target Pb^{2+}, the substrate strand is cleaved into two fragments, while the enzyme strand is exposed on the electrode. With the aid of helper DNA, Au–Pd bimetallic nanoparticles labeled with G-rich DNA strand (G-DNA) are conjugated onto the electrode through the hybridization reaction. Finally, hemin/G-quadruplex-based DNAzyme is formed upon addition of hemin, which can catalyze the reduction of H_2O_2 generated from NADH in the presence of O_2 with the porous Au–Pd bimetallic nanoparticles. The electronic signal is achieved by using thionine as electron mediator. The current is indirectly dependent on concentration of target Pb^{2+} in the sample. By calculating the variation in the cathodic current, we can quantitatively evaluate the level of the analyte with high sensitivity.

2. Experimental

2.1. Reagent and chemicals

Tris (2-carboxyethyl) phosphine hydrochloride (TCEP), 6-mercapto-1-hexanol (MCH) and hemin were acquired from Tokyo Chem. Industry (Japan). Ascorbic acid, $HAuCl_4 \cdot 4H_2O$, $PdCl_2$ and $Pb(OAc)_2 \cdot 3H_2O$ were purchased from Sinopharm Chem. Re. Co., Ltd. (Shanghai, China). Hexadecylpyridinium chloride (HDPC) was achieved from Aladdin Inc. (Shanghai, China). Thionine was gotten from Sigma-Aldrich (Shanghai, China). Reduced NADH and all the oligonucleotides used in this work were obtained from Dingguo Biotechnol. Co., Ltd. (Beijing, China). The sequences of the oligonucleotides are listed as follows [*Note*: the sequences of oligonucleotides were designed consulting to the literatures (Liu and Lu, 2004; Pelossof et al., 2012), and the 'rA' in the substrate stand referred to the cleavage site of Pb^{2+}].

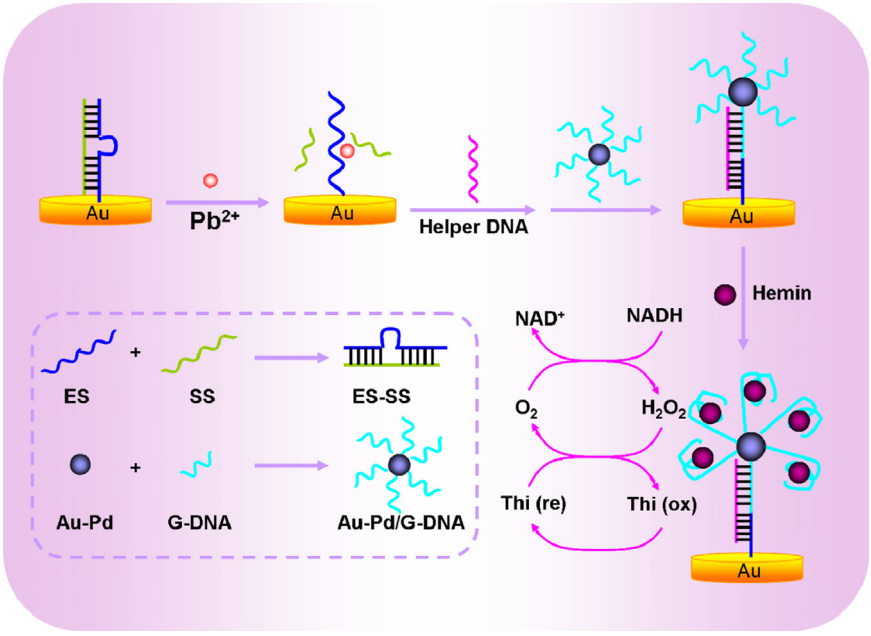

Scheme 1. Schematic illustration of the electrochemical DNA biosensor for quantitative monitoring of Pb^{2+} concentration based on synergetic catalysis of hemin/G-quadruplex DNAzyme and porous Au–Pd hybrid nanostructures (ES: enzyme strand; SS: substrate strand; ES-SS: Pb^{2+}-specific DNAzyme; Au–Pd: Au–Pd bimetallic hybrid nanostructure; G-DNA: G-rich DNA strand; Au–Pd/G-DNA: G-DNS-labeling Au–Pd).

Enzyme strand (ES): 5′-SH-TTTCATCTCTTCTCCGAGCCGGTC-GAAATAGTGAGT-3′

Substrate strand (SS): 5′-ACTCACTAT**rA**GGAAGAGATG-3′

G-rich DNA (G-DNA): 5′-GGGTTGGGCGGGATGGGTTT-SH-3′

Helper DNA: 5′-CCCATCCCGCCCAACCCACTCACTATTTC-GACCGGCTCGGAGAAGAGATG-3′

All other reagents were of analytical grade and used as received without further purification. Ultrapure water obtained from a Millipore water purification system (18.2 MΩ cm^{-1}, Milli-Q) was used in all runs. Pb^{2+} stock solution was prepared by dissolving Pb $(OAc)_2 \cdot 3H_2O$ in 10% HOAc, and further dilution was performed with 50 mM Tris-acetate buffer solution (0.5 M NaCl, pH 8.2). Phosphate-buffered saline (PBS) solution was the product of Sigma.

2.2. Synthesis of Au–Pd porous bimetallic nanostructures

Prior to synthesis, a 10-mM H_2PdCl_4 aqueous solution was prepared by dissolving 44.5-mg $PdCl_2$ into 25 mL of 20-mM HCl in a boiling water bath. Thereafter, porous Au–Pd bimetallic nanoparticles were synthesized according to the literature with minor modification (Huang et al., 2013). Briefly, H_2PdCl_4 aqueous solution (10 mM, 0.5 mL), $HAuCl_4$ aqueous solution (10 mM, 0.1 mL) and HDPC (0.02 g) were initially added to 5-mL ultrapure water. The resultant mixture was sonicated to obtain a homogeneous suspension. Afterwards, 0.4 mL of freshly prepared ascorbic acid aqueous solution (0.1 M) was rapidly injected into the mixture under gentle shaking. The mixture was kept undisturbed for 120 min at 35 °C. Finally, the product (*i.e.*, Au–Pd bimetallic hybrid nanostructures) was collected by centrifugation and washed twice with distilled water. The obtained Au–Pd bimetallic nanostructures were redispersed in 2 mL deionized water and stored at 4 °C for further use. For comparison, gold nanoparticles (AuNPs) and palladium nanoparticles (PdNPs) were synthesized by using the similar method.

2.3. Preparation of Pb^{2+}-specific DNAzyme sensor and G-DNA-labeled Au–Pd nanoparticles

Before modification, thiolated enzyme strand and G-rich DNA were left into 10 mM TCEP for 60 min at room temperature to reduce the possibly formed disulfide bond, respectively. To form Pb^{2+}-specific DNAzyme, a mixture containing 1.0-μM enzyme strand and 1.0-μM substrate strand was prepared in 1.0-mL PBS (10 mM, pH 7.4) (*i.e.*, formation of ES-SS). Afterwards, the mixture was incubated at 65 °C for 10 min, and then cooled to room temperature for further hybridization for 12 h under gentle shaking. The obtained ES-SS solution was stored at 4 °C for further use. To obtain G-DNA-labeled Au–Pd bimetallic nanoparticles (designated as Au–Pd/G-DNA), 10-μM G-DNA and 0.3 mL of the above-prepared Au–Pd porous bimetallic nanoparticles were mixed into 1.2-mL PBS (10 mM, pH 7.4), and kept at room temperature for 6 h under gentle shaking. After being separated by centrifugation, the obtained precipitate was dispersed in 1.0 mL of pH 7.4 PBS (10 mM) for target Pd^{2+} detection.

Next, a gold electrode with 2.0 mm in diameter was initially polished on a microcloth with alumina slurry (0.3 and 0.05 μm), and then washed by sonication in acetone, ethanol and ultrapure water for 5 min in sequence. The polished electrode was further cleaned through voltammetric scanning in 0.5 M H_2SO_4 from −0.3 V to +1.5 V until a steady-state cyclic voltammogram was obtained. After that, the resulting electrode was washed with ultrapure water thoroughly, dried with N_2, and immersed into the above-prepared ES-SS solution for 6 h at 4 °C. After being rinsed with pH 7.4 PBS (10 mM), the modified electrode was dipped into 1.0 mM MCH for 60 min to block the possible active sites on the electrode. Finally, the as-prepared Pb^{2+}-specific DNAzyme sensor was stored at 4 °C when not in use.

2.4. Electrochemical measurements toward target Pb^{2+}

Scheme 1 gives schematic illustration of the as-prepared DNA sensor for electrochemical detection of target Pb^{2+} based on synergetic catalysis of hemin/G-quadruplex DNAzyme and porous Au–Pd hybrid nanostructures. Initially, the sensor was reacted with target Pb^{2+} with different concentrations for 90 min at room temperature. During this process, Pb^{2+}-mediated DNAzyme acquired its cleavage activity, and the substrate strand was cleaved into two pieces at the 'rA' site, accompanying the release of enzyme strand. Afterwards, 5-μL helper DNA (1.0 μM) was dropped onto the electrode to hybridize with the exposed enzyme strand. Following that, the resulting electrode was further incubated with the above-prepared Au–Pd/G-DNA suspension and 2-μM hemin solution (30 min at room temperature) in turn. After each step, the modified electrode was washed with pH 7.4 PBS. Prior to electrochemical measurement, the detection system should be deaerated with nitrogen for 20 min to avoid the oxidation of thionine. However, it was unnecessary to keep over with nitrogen during the detection process because a small amount of oxygen participated in the reaction of NADH in this system. All the electronic measurements were carried out on an AutoLab electrochemical workstation (Eco Chemie, The Netherlands) with a conventional three-electrode system including a modified gold working electrode, a platinum-wire auxiliary electrode and an Ag/AgCl reference electrode. Differential pulse voltammetry (DPV) was performed in PBS (0.1 M, pH 7.4) containing 2.0-mM NADH and 30-μM thionine within the applied potential range from +0.1 V to −0.5 V. Electrochemical impedance spectroscopy (EIS) was carried out in PBS (0.1 M, pH 7.4) containing 0.1 M KCl and 10 mM $[Fe(CN)_6]^{3-/4-}$. Analyses are always made in triplicate.

2.5. Monitoring of real samples with inductively coupled plasma mass spectrometry (ICP-MS)

ICP-MS measurements were carried out by using a quadrupole ICP-MS spectrometer 7700 X (Agilent Technology) with a quartz concentric nebulizer (1.0 mL). For the ICP-MS method, the sample solutions were prepared from certified stock multi-elemental 1.11×10^{-2} mol L^{-1} solutions SPEX (Jobin Yvon). The operation conditions were as follows (RF power: 1500 W; Plasma gas flow: 15 L min^{-1}; Makeup gas flow: 0.9 L min^{-1}; Carrier gas flow: 1.1 L min^{-1}; Interface vacuum: 1.0 hPa, Analyzer vacuum: 3.8×10^{-7} hPa; Dwell time: 10 ms/element; Ion collecting mode: Pulse counting).

3. Results and discussion

3.1. Characterizations of Au–Pd bimetallic nanostructures and sensor fabrication process

High-resolution transmission electron microscope (HRTEM, FEI Titan 80-300, Hillsboro, USA) and energy-dispersive X-ray (EDX, FEI Titan^3 electron microscope, Hillsboro, USA) spectroscope were first utilized to characterize the as-prepared Au–Pd bimetallic nanoparticles, respectively. Fig. 1A shows the typical HRTEM image of Au–Pd hybrid nanostructures. Au–Pd bimetallic nanoparticles were monodispersed and porous. The average size was estimated to be about 60 nm, which was in accordance with the result obtained from dynamic light scatter (DLS; Zetasizer Nano S90, Malvern, London, U.K.) (Fig. 1A, right inset). The analysis of EDX pattern for the hybrid nanostructures also indicated the existence of

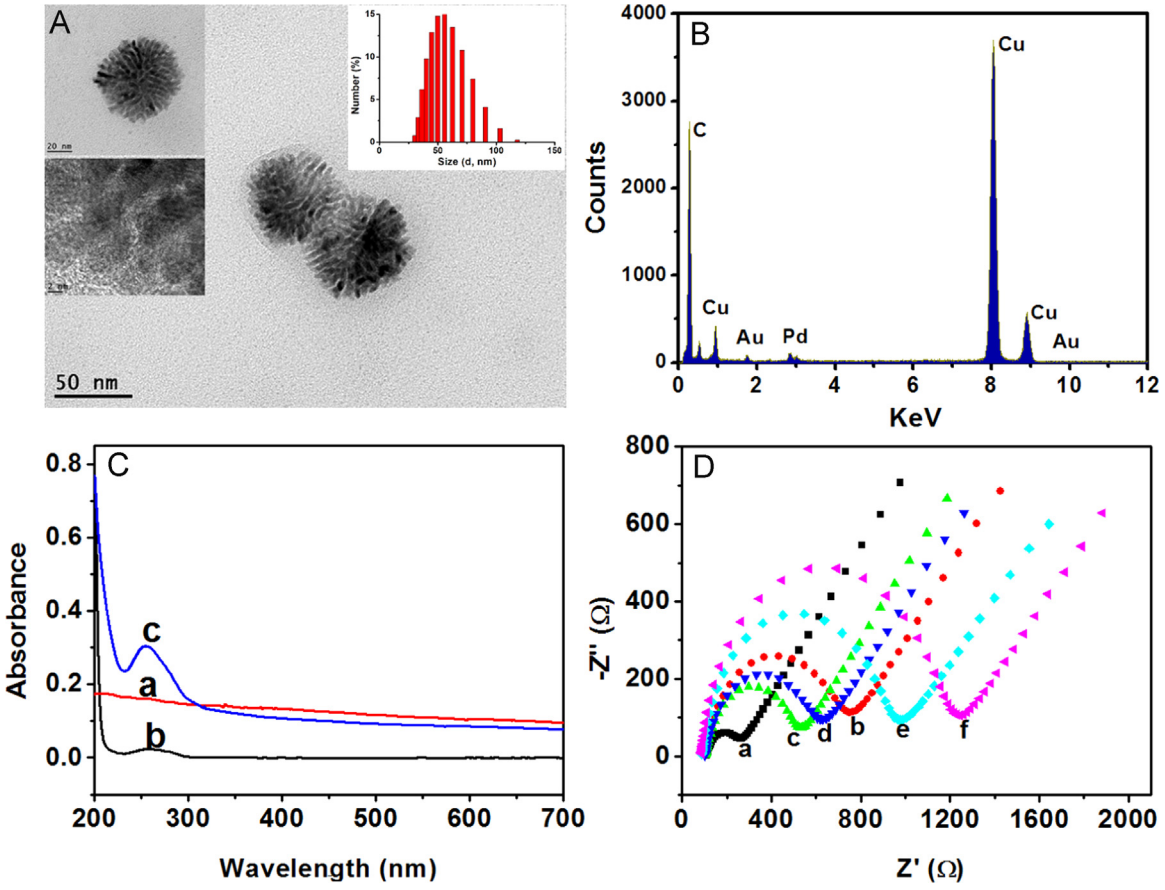

Fig. 1. (A) HRTEM image and (B) EDX pattern of the as-prepared Au–Pd porous bimetallic nanoparticles [insets in (A): magnification images (left) and DLS data (right)]; (C) UV–vis spectra of (a) Au–Pd bimetallic nanoparticles, (b) G-DNA and (c) G-DNA-labeled Au–Pd bimetallic nanoparticles; (D) Nyquist diagrams of (a) gold electrode, (b) electrode '*a*'+ES-SS+MCH, (c) electrode '*b*'+target Pb^{2+}, (d) electrode '*c*'+helper DNA, (e) electrode '*d*'+Au–Pd/G-DNA and (f) electrode '*e*'+hemin in PBS (0.1 M, pH 7.4) containing 0.1 M KCl and 10 mM $[Fe(CN)_6]^{3-/4-}$ with the range from 0.1 Hz to 10^5 Hz at an alternate voltage of 5 mV.

Au and Pd elements (Fig. 1B). On the basis of these results, we might make a conclusion that the porous Au–Pd bimetallic nanoparticles could be successfully synthesized by our designed strategy. Further, UV–vis absorbance spectroscope (UV 1102, Techcomp, China) was employed to confirm the binding of thiolated G-DNA and Au–Pd bimetallic nanoparticles. No absorption peaks were observed at Au–Pd bimetallic nanoparticles (Fig. 1C, curve '*a*'), which was another evidence for the successful synthesis of Au–Pd hybrid nanostructures (Ferrer et al., 2007; Zhan et al., 2011). When the as-synthesized Au–Pd bimetallic nanostructures were incubated with G-DNA molecules, however, an obvious characteristic adsorption peak at 260 nm was appeared (Fig. 1C, curve '*c*'). Compared with curve '*b*' in Fig. 1C, the peak derived from the labeled G-DNA. Hence, the as-prepared Au–Pd bimetallic nanoparticles could be used for the conjugation of thiolated G-DNA molecules through the Au–S bond.

Next, electrochemical impedance spectroscopy (EIS) was employed for investigation of the sensor fabrication process after each step in pH 7.4 PBS (0.1 M) containing 0.1 M KCl and 10 mM $[Fe(CN)_6]^{3-/4-}$ (Fig. 1D). The Nyquist plots were utilized to calculate the electron-transfer resistance (Zhang et al., 2008). After ES-SS-based Pb^{2+}-specific DNAzyme was assembled to the cleaned gold electrode, the diameter of the semicircle increased obviously (curve '*b*') in comparison with that of bare gold electrode (curve '*a*'), indicating that the double-stranded DNA hindered the electron transfer. In contrast, the resistance decreased after the as-prepared sensor reacted with target Pb^{2+} (curve '*c*') because of the cleavage of substrate strand and the release of enzyme strand. With hybridization of the enzyme strand with helper DNA (curve '*d*'), however, the resistance increased again, especially when Au–Pd/G-DNA was conjugated to help DNA-modified electrode (curve '*e*'). The results suggested that G-DNA-labeled Au–Pd hybrid nanoparticles could be immobilized on the electrode through helper DNA. Finally, the resulting electrode reacted with hemin, and the resistance increased (curve '*f*'), indicating that hemin was bound to G-DNA molecules and formed a hemin/G-quadruplex-based DNAzyme. The formed hemin/G-quadruplex increased the steric hindrance and hindered the electron transfer of $[Fe(CN)_6]^{3-/4-}$, thereby leading to an increase in the resistance. These changes in the electron transfer resistance verified the successful fabrication of the biosensor, which could be preliminarily applied for the detection of target Pb^{2+}.

3.2. Feasibility investigation and comparative study

To elucidate the feasibility of our designed strategy for Pb^{2+} detection, the electrochemical characteristics of the as-prepared sensors were studied in the absence and presence of target Pb^{2+} (1.0 nM Pb^{2+} used in this case) using differential pulse voltammetry (DPV), respectively (Fig. 2A). Curve '*a*' gives the background signal of the newly prepared Pb^{2+}-specific sensor in pH 7.4 PBS containing 2.0 mM NADH and 30 μM thionine. The peak current derived from the added thionine in the supporting electrolyte. Compared with curve''*a*', the peak current of the sensor was not almost changed in the absence of target Pb^{2+}, indicating that the prepared Au–Pd/G-DNA could not non-specifically adsorb to the sensor. In contrast, the peak current largely increased upon addition of 1.0 nM target Pb^{2+} into the incubation solution (curve '*c*').

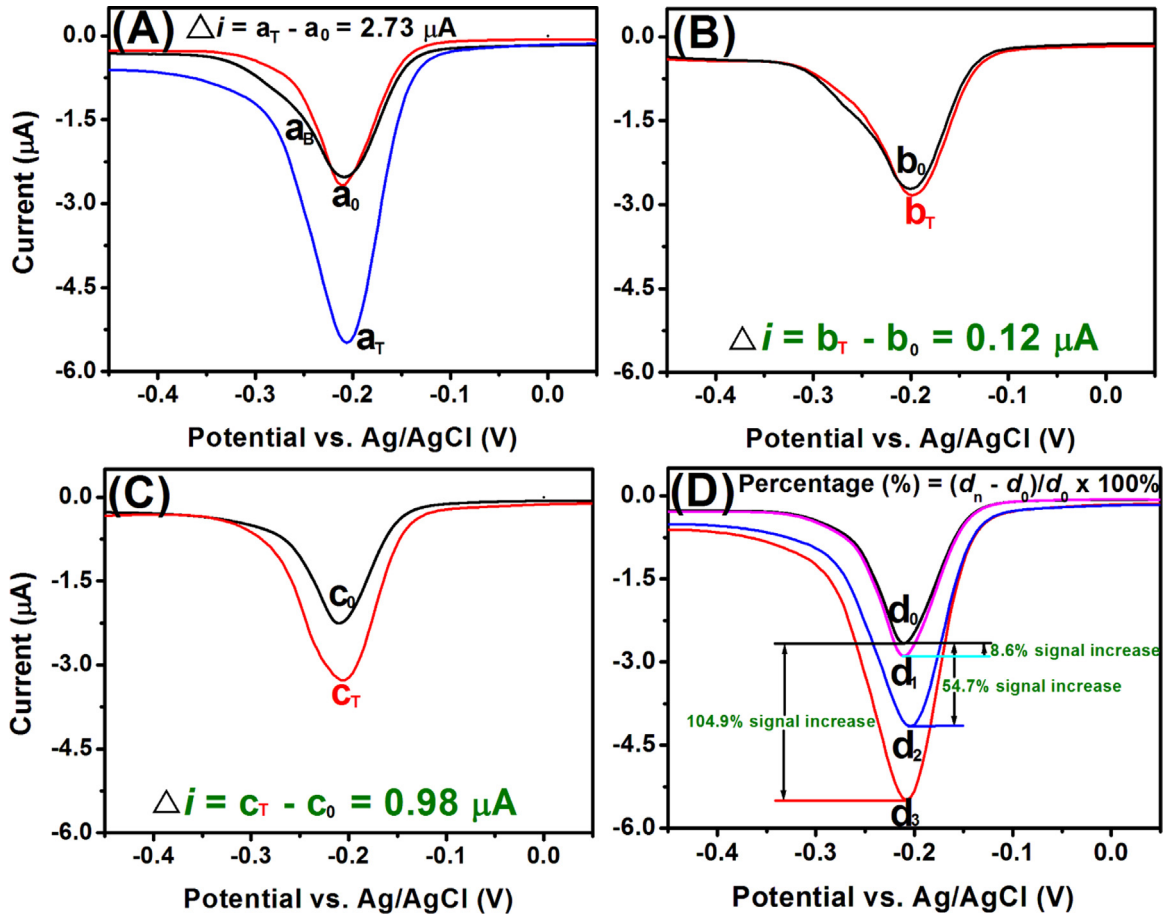

Fig. 2. DPV responses of Pb^{2+}-specific DNAzyme-modified electrode in the absence (a_0,b_0,c_0) and presence (a_T,b_T,c_T) of 1.0 nM target Pb^{2+} by using different strategies: (A) help DNA+Au–Pd/G-DNA+hemin, (B) help DNA+Au–Pd+hemin and (C) help DNA+G-DNA+hemin; and (D) DPV responses of the newly prepared sensor toward 1.0 nM target Pb^{2+} by using variously labeled strategies: (d_1) PdNP/G-DNA, (d_2) AuNP/G-DNA and (d_3) Au–Pd/G-DNA. The assay was carried out in pH 7.4 PBS (0.1 M) containing 2.0 mM NADH and 30 μM thionine. Curve 'a_B' and curve 'd_0' represent DPV responses of the newly prepared Pb^{2+}-specific DNAzyme-modified electrode.

The results also proved that the change in the electronic signal originated from the interaction between target Pb^{2+} and ES-SS complex, which could be preliminarily used for the detection of Pb^{2+}.

Logically, another question arises to whether the strong electrochemical signal depended on the as-synthesized Au–Pd/G-DNA. To demonstrate this issue, DPV responses of using Au–Pd and G-DNA alone were monitored in the absence and presence of target Pb^{2+} in pH 7.4 PBS containing 2.0 mM NADH and 30 μM thionine (Fig. 2B and C). As shown in Fig. 2B, the DPV peak current of using the unmodified Au–Pd bimetallic nanoparticles was almost the same whether target Pb^{2+} was present or not in the incubation solution. The results indicated that the unmodified Au–Pd bimetallic nanostructures could not be conjugated to the sensor in the absence of G-DNA. Although use of G-DNA could cause the increase in the peak current of the sensor (Fig. 2C), the signal was relatively smaller in comparison with that in Fig. 2A. The reason was ascribed to the fact that the formation of hemin/G-quadruplex-based DNAzyme could induce the progression of the catalytic reaction, thus resulting in the signal increase.

To further elucidate the advantages of bimetallic nanoparticles over their signal-component counterparts, three types of labeling strategies including Au–Pd/G-DNA, AuNP/G-DNA and PdNP/G-DNA were used for the detection of 1.0 nM Pb^{2+} (used as an example) by using the same assay protocol with the same-batch sensors. The evaluation was based on the change in the current relative to background signal. As shown in Fig. 2D, use of AuNP/G-DNA could cause a 54.7 ± 2.1% signal increase (curve 'd_2' *vs.* curve 'd_0'), while the signal only increased 8.6 ± 0.9% (curve 'd_1' *vs.* curve 'd_0'). We suspected that the relatively small increase in the current might be ascribed to the facts that the thiolated G-DNA could be readily conjugated on the AuNP, while G-DNA was difficultly labeled onto the PdNP. Significantly, the signal could reach a 104.9 ± 7.8% increase in comparison with the background signal by using Au–Pd/G-DNA. Experimental results indicated that the detectable signal with Au–Pd/G-DNA was 1.9 times of AuNP/G-DNA [*i.e.*, $(d_3-d_0)\div(d_2-d_0)$] and 13.8 times of PdNP/G-DNA [*i.e.*, $(d_3-d_0)\div(d_1-d_0)$], respectively. Several possible explanations might be attributed to the results: (i) Au–Pd bimetallic nanoparticles could exhibited high surface-to-volume ratio for the conjugation of G-DNA (Wang et al., 2013; Yuan et al., 2014), and (ii) the doped palladium nanoparticles in the Au–Pd hybrid nanostructures could be utilized as an enzymatic mimic for the progression of catalytic reaction. Therefore, the as-synthesized porous Au–Pd bimetallic nanostructures could be used for the signal amplification of Pb^{2+} sensing strategy.

3.3. Optimization of experimental conditions

Generally speaking, experimental conditions have the effects on the analytical performance of the sensing strategy. To obtain an optimal electrochemical signal, experimental conditions including NADH concentration, thionine concentration, hemin concentration and cleavage time of Pb^{2+}-mediated DNAzyme were studied. NADH concentration has a close relationship with the amount of the produced H_2O_2. Thus, NADH concentration could affect the

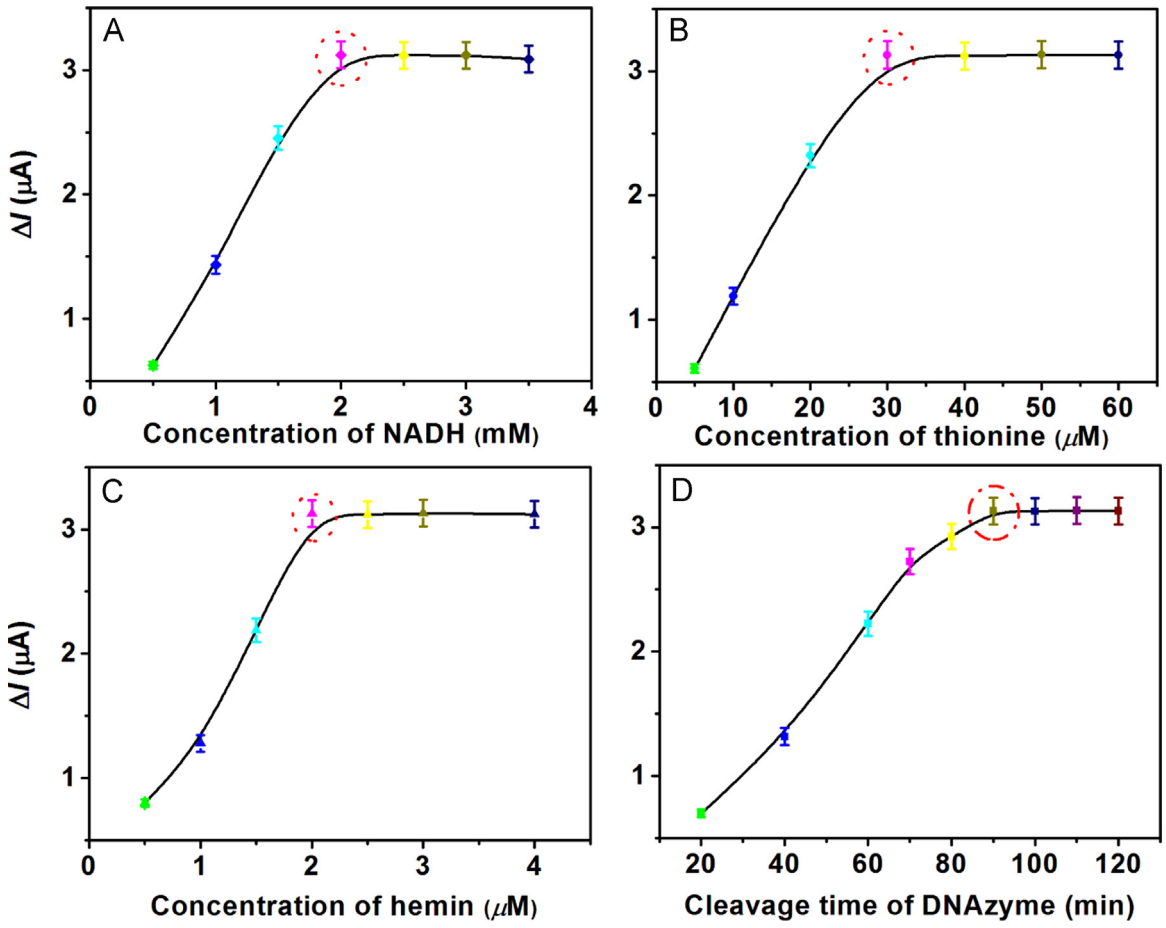

Fig. 3. Effects of (A) NADH concentration, (B) thionine concentration, (C) hemin concentration and (D) cleavage time of DNAzyme on the electrochemical signal of the developed sensing platform by using 1.0 nM Pb^{2+} used as an example.

detectable signal of our system. As shown in Fig. 3A. The DPV peak current variation (ΔI) ($\Delta I = I_0 - I$; I_0 presents the background current, while I was defined as the current toward 1.0 nM target Pb^{2+} under different conditions) increased with the increasing NADH concentrations, and reached a plateau when NADH concentration was over 2 mM. Therefore, 2 mM was chosen as the optimal NADH concentration. As the electron mediator, thionine plays an important role in the detection process, and its concentration may also affect the response signal. ΔI increased with the increase of thionine concentration, and tended to level off at 30 μM (Fig. 3B). So, the optimal NADH concentration was chosen at 30 μM. The concentration of hemin had a great influence on the formation of hemin/G-quadruplex-based DNAzyme. As seen from Fig. 3C, ΔI reached a plateau after hemin concentration was increased to 2 μM. Thus, 2 μM was chosen as the optimal hemin concentration. The cleavage of Pb^{2+}-specific DNAzyme was also the key step in the whole Pb^{2+} sensing process. Fig. 3D gives the relationship between ΔI and cleavage time of the DNAzyme. ΔI increased with

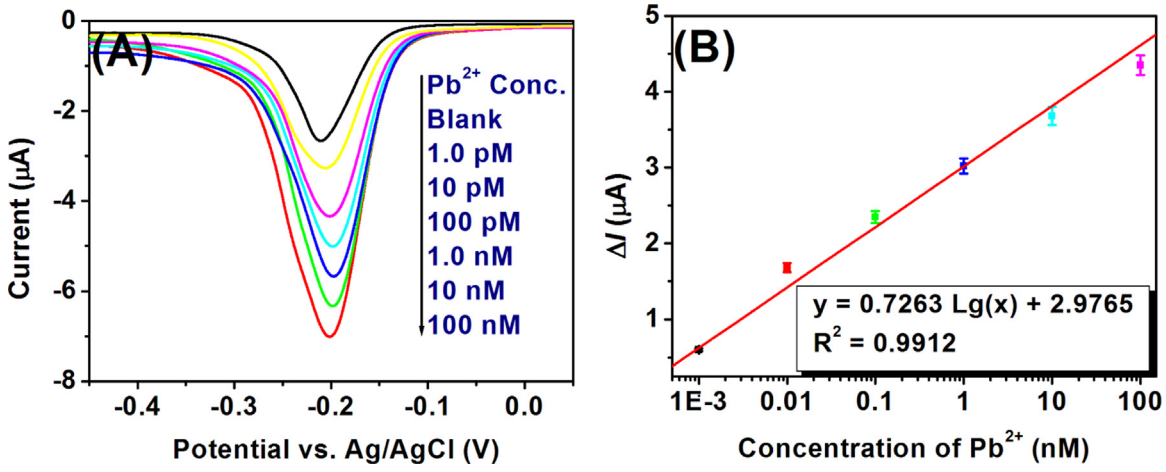

Fig. 4. (A) DPV responses of the electrochemical sensing platform toward different Pb^{2+} concentrations in pH 7.4 PBS (0.1 M) containing 2.0 mM NADH and 30 μM thionine, and (B) the corresponding calibration plots.

the increasing cleavage time and achieved its maximum value after 90 min. Hence, 90 min was chosen as the optimal cleavage time.

3.4. Dose-response curves toward Pb^{2+} standards

Under the optimal conditions, the sensitivity and dynamic range of the developed sensing platform towards target Pb^{2+} were studied by using DPV in PBS (0.1 M, pH 7.4) containing 2 mM NADH and 30 μM thionine. The DPV curves in Fig. 4A showed that the peak currents gradually increased with the increasing target Pb^{2+} concentrations. The reason could be the fact that target Pb^{2+} could cause the cleavage of substrate strands and released the free enzyme strands. In this case, more G-DNA-labeled Au–Pd bimetallic nanoparticles could be captured onto enzyme strand-modified electrode *via* helper DNA to form hemin/G-quadruplex-based DNAzyme, thus enhancing the peak current. The ΔI was linearly dependent on the logarithm of Pb^{2+} concentration in the dynamic range of 1.0 pM to 100 nM with a correlation coefficient of 0.9956 (*i.e.*, r) (Fig. 4B). The limit of detection (LOD) was found at 0.34 pM estimated at the signal-to-noise ratio of 3. Obviously, the LOD of our system was comparable with those of Pb^{2+}-dependent DNAzyme-based evanescent wave-induced emission biosensing platform (LOD: 1.0 nM) (Wang et al., 2015b), silica microsphere-based fluorescent sensor (LOD: 36 nM) (Ding et al., 2015), GeneFinder (TM)-based fluorescent detection (LOD: 2.62 ppb) (Zhan et al., 2015), graphene oxide-based electrochemical detection (LOD: 7.8 pM) (Wang et al., 2015a), electrospun carbon nanofiber-modified electrodes for stripping voltammetry (LOD: 0.9 nM) (Zhao et al., 2015), $Ru(bpy)_3^{2+}$-based electrochemiluminescence sensor (LOD: 0.1 nM) (Zhu et al., 2009), diaminoterthiophene-based chronocoulometric sensor (LOD: 1.9 ng mL^{-1}) (Choi et al., 2015), hybridization chain reaction-based electrochemical method (LOD: 37 pM) (Zhuang et al., 2013) and electrochemiluminescence resonance energy transfer system (LOD: 0.35 pM) (Lei et al., 2015). Therefore, the proposed sensing platform for Pb^{2+} detection based on DNAzymes and Au–Pd porous bimetallic nanoparticles exhibited a low detection limit.

3.5. Specificity, reproducibility and stability

The specificity of the sensing strategy was investigated by challenging the system against other metal ions including Hg^{2+}, Cu^{2+}, Zn^{2+}, Fe^{2+}, Cd^{2+}, Mg^{2+}, Ca^{2+} and Fe^{3+}. As shown in Fig. 5A, only target Pb^{2+} caused a significant variation (ΔI) in the DPV peak current although the concentrations of other tested ions were larger than that of Pb^{2+}. Moreover, we further challenged the biosensor with Pb^{2+} in the coexistence of other metal ions. As shown in Fig. 5B, the coexistence of other tested metal ion almost had no effect on the response of this biosensor to Pb^{2+}. These results clearly demonstrated that this sensing platform was highly selective for the target Pb^{2+}.

The reproducibility of the sensing platform was estimated by evaluating the coefficient of variation (CV) for the intra-assay or inter-assay. Experimental results indicated that the CVs of the assays with the same-batch sensors were 6.8%, 7.6% and 8.4% at 10 pM, 1.0 nM, and 100 nM Pb^{2+}, respectively. The batch-to-batch reproducibility was also investigated and the CVs were 9.2%, 9.8% and 8.9% at the above-mentioned three concentrations, respectively. Additionally, the stability of the as-prepared sensor was also studied on a 30-day period. The sensors were stored at 4 °C and measured intermittently (every 3–5 days). They preserved 90.2% of the initial response after a storage period of 18 days. These results revealed that the reproducibility and stability of this method was acceptable.

3.6. Analysis of real samples

To investigate the application potential of the developed sensing strategy in environmental analysis, the as-prepared sensors were first applied for the detection of target Pb^{2+} in water samples, which were obtained from the local Minjiang River (Fuzhou, China). Three samples were prepared by spiking Pb^{2+} standards into blank water. Experimental results indicated that the recoveries were 95.8–109%. In addition, 5 contaminated sewage samples (*Note*: these samples were prepared through mixture of tap water with different-volume battery electrolyte matrices) were monitored using the developed Pb^{2+} sensor, and the obtained results were compared with the referenced values from ICP-MS. The Pb^{2+} contents ($n=3$) toward five samples were 3.8 ± 0.4 nM, 27.4 ± 1.3 nM, 0.43 ± 0.08 nM, 13.1 ± 1.6 nM and 37.8 ± 3.4 nM for the developed Pb^{2+} sensor, and 4.1 ± 0.5 nM, 26.4 ± 0.9 nM, 0.48 ± 0.07 nM, 13.9 ± 1.3 nM and 36.2 ± 2.9 nM for ICP-MS, respectively. The regression equation between two method could be fitted to $y=0.9479\ x+0.5703$ ($R^2=0.9987$, $n=5$). The slope was close to unit '1'. Hence, no significant differences between two methods were encountered, indicating that the designed sensing platform could be applied for the detection of target Pb^{2+} in environmental water samples.

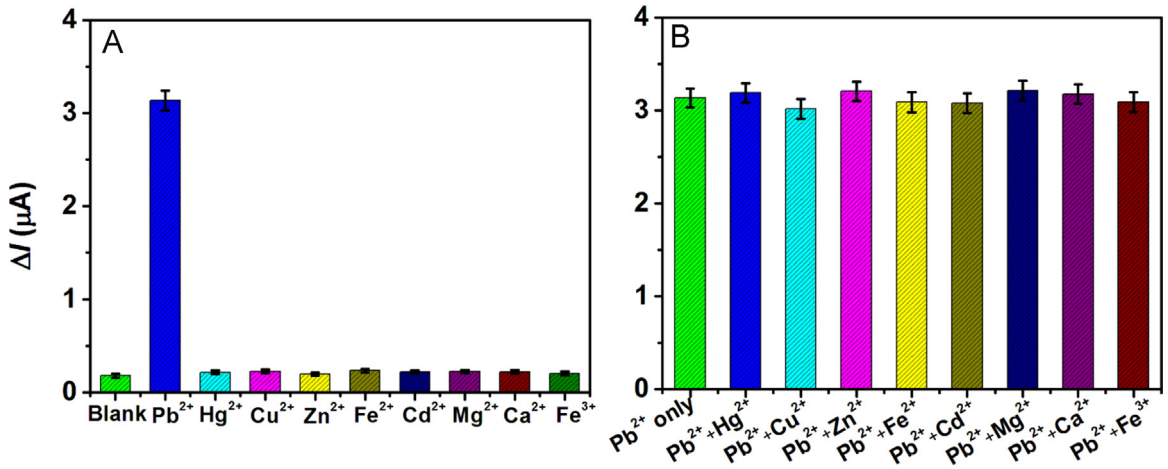

Fig. 5. The specificity of the electrochemical sensing platform toward target Pb^{2+} against Hg^{2+}, Cu^{2+}, Zn^{2+}, Fe^{2+}, Cd^{2+}, Mg^{2+}, Ca^{2+} and Fe^{3+}: (A) for individual metal ion alone and (B) target+co-existed ion (*Note*: 1.0 nM Pb^{2+} and 100 nM interfering ions used in all the cases).

4. Conclusions

In summary, we have successfully developed a sensitive sensing platform for specific Pb^{2+} detection based on synergetic catalysis of Au–Pd bimetallic nanoparticles and DNAzyme. Use of porous Au–Pd nanostructures increased the surface coverage of the nanostructures, and enhanced the labeling amount of G-rich DNA molecules. Compared with conventional Pd^{2+} sensing strategies and our previous reports (Zhu et al., 2009; Zhuang et al., 2013), highlights of this works could be summarized as follows: (i) hemin/G-quadruplex-based DNAzyme not only acted as NADH oxidase, but also peroxidase-like mimics; (ii) the substrate (H_2O_2) of peroxidase was *in situ* produced from NADH through Au–Pd bimetallic nanoparticles, thereby resulting in the signal amplification; (iii) the doped palladium could catalyze H_2O_2 reduction to some extent; and (iv) introduction of help DNA in the system could efficiently decrease the non-specific adsorption. Because of simple operation, low cost and easy preparation, the methodology demonstrated in this work provided a promising scheme for the detection of target Pb^{2+}. By changing the sequences of enzyme/substrate strands to form different metal ions-mediated DNAzymes, importantly, the sensing platform can be utilized for the detection of other metal ions such as Zn^{2+}, Cu^{2+} and Hg^{2+}.

Acknowledgments

This work was financially supported by the National Natural Science Foundation of China (41176079 and 21475025), the National Science Foundation of Fujian Province (2014J07001), Key Science Project (Type A) of the Fujian Provincial Department of Education, China (JA12021) and the Program for Changjiang Scholars and Innovative Research Team in University (IRT1116).

References

Bontidean, I., Ahlqvist, J., Mulchandani, A., Chen, W., Bae, W., Mehra, R.K., Mortari, A., Csöregi, E., 2003. Biosens. Bioelectron. 18, 547–553.
Bukar, N., Zhao, S.S., Charbonneau, D.M., Pelletier, J.N., Masson, J.F., 2014. Chem. Commun. 50, 4947–4950.
Cheng, L.C., Huang, J.H., Chen, H.M., Lai, T.C., Yang, K.Y., Liu, R.S., Hsiao, M., Chen, C. H., Her, L.J., Tsai, D.P., 2012. J. Mater. Chem. 22, 2244–2253.
Choi, S., Kim, D., Jung, O., Shim, Y., 2015. Anal. Chim. Acta 892, 77–84.
Chung, W., Heddi, B., Schmitt, E., Lim, K., Mechulam, Y., Phan, A., 2015. Proc. Natl. Acad. Sci. 112, 2729–2733.
Ding, Y., Zhu, W., Xu, Y., Qian, X., 2015. Sens. Actuators B 220, 762–771.
Dong, J., Fang, Q., He, H., Zhang, Y., Xu, J., Sun, Y., 2015. Microchim. Acta 182, 653–659.
Dwivedi, C., Chaudhary, A., Gupta, A., Nandi, C.K., 2015. ACS Appl. Mater. Interfaces 7, 5039–5044.
Ferrer, D., Torres-Castro, A., Gao, X., Sepulveda-Guzman, S., Ortiz-Mendez, U., Jose-Yacaman, M., 2007. Nano Lett. 7, 1701–1705.
Gao, C., Yu, X., Xu, R., Liu, J., Huang, X., 2012. ACS Appl. Mater. Interfaces 4, 4672–4682.
Gao, F., Goodman, D.W., 2012. Chem. Soc. Rev. 41, 8009–8020.
Ge, S., Liu, F., Liu, W., Yan, M., Song, X., Yu, J., 2014. Chem. Commun. 50, 475–477.
Golub, E., Freeman, R., Willner, I., 2011. Angew. Chem. Int. Ed. 50, 11710–11714.
Gui, R., Jin, H., 2013. Analyst 138, 7197–7205.
Guo, Y., Yang, G., Sun, X., Chen, H.Y., Xu, J.J., 2015. Chem. Commun. 51, 862–865.
Han, G., Feng, X., Chen, Z., 2014. Int. J. Electrochem. Sci. 10, 3897–3913.
He, H.Z., Leung, K.H., Yang, H., Chan, D.S.H., Leung, C.H., Zhou, J., Bourdoncle, A., Mergny, J.L., Ma, D.L., 2013a. Biosens. Bioelectron. 41, 871–874.
He, Y., Wang, X., Zhang, Y., Gao, F., Li, Y., Chen, H., Wang, L., 2013b. Talanta 116, 816–821.
Huang, X., Li, Y., Chen, Y., Zhou, E., Xu, Y., Zhou, H., Duan, X., Huang, Y., 2013. Angew. Chem. Int. Ed. 125, 2580–2584.
Kuo, S.Y., Li, H.H., Wu, P.J., Chen, C.P., Huang, Y.C., Chan, Y.H., 2015. Anal. Chem. 87, 4765–4771.
Lei, Y., Huang, W., Zhao, M., Chai, Y., Yuan, R., Zhuo, Y., 2015. Anal. Chem. 87, 7787–7794.
Li, C.L., Huang, C.C., Chen, W.H., Chiang, C.K., Chang, H.T., 2012. Analyst 137, 5222–5228.
Li, M., Kong, Q., Bian, Z., Ma, C., Ge, S., Zhang, Y., Yu, J., Yan, M., 2015. Biosens. Bioelectron. 65, 176–182.
Li, W., Qiang, W., Li, J., Li, H., Dong, Y., Zhao, Y., Xu, D., 2014. Biosens. Bioelectron. 51, 219–224.
Lin, Y., Ren, J., Qu, X., 2014. Accounts Chem. Res. 47, 1097–1105.
Liu, J., Lu, Y., 2004. Chem. Mater. 16, 3231–3238.
Liu, S., Cheng, C., Liu, T., Wang, L., Gong, H., Li, F., 2015. Biosens. Bioelectron. 63, 99–104.
Ma, D., Zhang, Z., Wang, M., Lu, L., Zhong, H., Leung, C., 2015. Chem. Biol. 22, 812–828.
Mitrano, D.M., Barber, A., Bednar, A., Westerhoff, P., Higgins, C.P., Ranville, J.F., 2012. J. Anal. At. Spectrom. 27, 1131–1142.
Muralikrishna, S., Sureshkumar, K., Varley, T.S., Nagaraju, D.H., Ramakrishnappa, T., 2014. Anal. Methods 6, 8698–8705.
Naghmush, A.M., Pyrzyńska, K., Trojanowicz, M., 1995. Talanta 42, 851–860.
Pelossof, G., Tel-Vered, R., Willner, I., 2012. Anal. Chem. 84, 3703–3709.
Poon, K.C., Tan, D.C., Vo, T.D., Khezri, B., Su, H., Webster, R.D., Sato, H., 2014. J. Am. Chem. Soc. 136, 5217–5220.
Qian, Z.S., Shan, X.Y., Chai, L.J., Chen, J.R., Feng, H., 2015. Biosens. Bioelectron. 68, 225–231.
Ruttkay-Nedecky, B., Kudr, J., Nejdl, L., Maskova, D., Kizek, R., Adam, V., 2013. Molecules 18, 14760–14779.
Shen, L., Chen, Z., Li, Y., He, S., Xie, S., Xu, X., Liang, Z., Meng, X., Li, Q., Zhu, Z., Li, M., Le, X.C., Shao, Y., 2008. Anal. Chem. 80, 6323–6328.
Tsekenis, G., Filippidou, M.K., Chatzipetrou, M., Tsouti, V., Zergioti, I., Chatzandroulis, S., 2015. Sens. Actuators B 208, 628–635.
Wang, M., Zhang, S., Ye, Z., Peng, D., He, L., Yan, F., Yang, Y., Zhang, H., Zhang, Z., 2015a. Microchim. Acta 182, 2251–2258.
Wang, R., Zhou, X., Shi, H., 2015b. Biosens. Bioelectron. 74, 78–84.
Wang, R., Wu, Z., Chen, C., Qin, Z., Zhu, H., Wang, G., Wang, H., Wu, C., Dong, W., Fan, W., Wang, J., 2013. Chem. Commun. 49, 8250–8252.
Yuan, L., Tu, W., Bao, J., Dai, Z., 2014. Anal. Chem. 87, 686–692.
Yuan, Y., Chai, Y., Yuan, R., Zhuo, Y., Gan, X., 2013. Chem. Commun. 49, 7328–7330.
Zhao, D., Wang, T., Han, D., Rusinek, C., Steckl, A., Heineman, W., 2015. Anal. Chem. 87, 9315–9321.
Zhan, G., Huang, J., Du, M., Abdul-Rauf, I., Ma, Y., Li, Q., 2011. Mater. Lett. 65, 2989–2991.
Zhan, S., Xu, H., Zhang, D., Xia, B., Zhan, X., Wang, L., Lv, J., Zhou, P., 2015. Biosens. Bioelectron. 72, 95–99.
Zhang, B., Chen, J., Liu, B., Tang, D., 2015a. Biosens. Bioelectron. 69, 230–234.
Zhang, P., Wu, X., Yuan, R., Chai, Y., 2015b. Anal. Chem. 87, 3202–3207.
Zhang, S., Xia, J., Li, X., 2008. Anal. Chem. 80, 8382–8388.
Zhang, Y., Fan, J., Nie, J., Le, S., Zhu, W., Gao, D., Yang, J., Zhang, S., Li, J., 2015c. Biosens. Bioelectron. 73, 13–18.
Zhang, Y., Wang, L., Tian, J., Li, H., Luo, Y., Sun, X., 2011. Langmuir 27, 2170–2175.
Zhu, X., Lin, Z., Chen, L., Qiu, B., Chen, G., 2009. Chem. Commun. 45, 6050–6052.
Zhuang, J., Fu, L., Xu, M., Zhou, Q., Chen, G., Tang, D., 2013. Biosens. Bioelectron. 45, 52–57.